THE JOURNAL OF PHYSICAL CHEMISTRY C

Article

pubs.acs.org/JPCC

Mapping the Ultrafast Changes of Continuous Shape Measures in Photoexcited Spin Crossover Complexes without Long-Range Order

S. E. Canton,*[,†] X. Zhang,[‡] M. L. Lawson Daku,[§] Y. Liu,[∥] J. Zhang,[⊥] and S. Alvarez[#]

[†]Department of Synchrotron Radiation Instrumentation, Lund University, P.O. Box 118, 22100 Lund, Sweden

[‡]X-ray Sciences Division, Argonne National Laboratory, 9700 South Cass Avenue, Argonne, Illinois 60439, United States

[§]Département de Chimie Physique, Université de Genève, Quai E. Ansermet 30, CH-1211 Genève 4, Switzerland

[∥]Centre for Analysis and Synthesis, Department of Chemistry, Lund University, S-22100 Lund, Sweden

[⊥]School of Environmental and Chemical Engineering, Tianjin Polytechnic University, Tianjin 300387, China

[#]Departament de Química Inorgànica and Institut de Química Teòrica i Computacional, Universitat de Barcelona, Martí i Franqués 1-11, 08028 Barcelona, Spain

ABSTRACT: Establishing a tractable yet complete reaction coordinate for the spin-state interconversion in d^4–d^7 transition metal complexes is an integral aspect of controlling the dynamics that govern their functionality. For spin crossover phenomena, the limitations of a single-mode approximation that solely accounts for an isotropic increase in the metal–ligand bond length have long been recognized for all but the simple octahedral monodentate Fe^{II} compounds. However, identifying the coupled deformations that also impact on the unimolecular rate constants remains experimentally and theoretically challenging, especially for samples that do not display long-range order or when crystallization profoundly alters the dynamics. Owing to the rapid progress in ultrafast X-ray absorption spectroscopy (XAS), it is now possible to obtain transient structural information in any physical phase with unprecedented details. Using picosecond XAS and DFT modeling, the structure adopted by the photoinduced high-spin state of solvated $[Fe(terpy)_2]^{2+}$ (terpy: 2,2′:6′,2″-terpyridine) has been recently established. Based on these results, the methodology of the continuous shape measure is applied to classify and quantify the short-lived distortion of the first coordination shell. The reaction coordinate of the spin-state interconversion is clearly identified as a double axial bending. This finding sets a benchmark for gauging the influence of first-sphere and second-sphere interactions in the family of Fe^{II} complexes that incorporate terpy derivatives. Some implications for the optimization of related photoactive Fe^{II} complexes are also outlined.

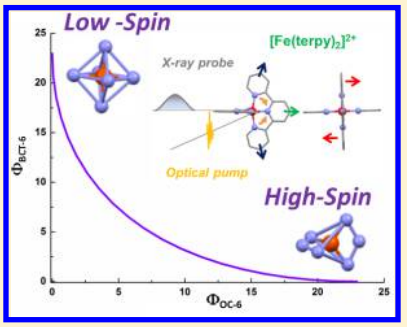

INTRODUCTION

Controlling the interconversion between the low-spin (LS) and the high-spin (HS) states in d^4–d^7 transition metal complexes of period 4 elements is central to their functionalization and their integration into emerging nanotechnologies.[1−6] Providing a comprehensive description of the switching dynamics requires uncovering the underlying reaction coordinate (RC). The promotion of electrons from a nonbonding t_{2g} orbital to an antibonding e_g orbital triggers an expansion of the first coordination sphere (FCS) in the HS state. The associated change in average metal–ligand (M–L) bond distance ΔR_{av} can be identified with the totally symmetric breathing mode. This parameter readily enters the expression of the rate constants when the spin crossover (SCO) transition is treated as a nonadiabatic radiationless process in the strong coupling limit.[7] However, a multimodal RC generally needs to be introduced for interpreting the electronic and structural dynamics,[8−11] so that the anisotropic deformations of the FCS must be explicitly incorporated into the mechanistic models of the SCO step.[12−16]

For the prominent family of quasi-octahedral (O_h) $[Fe^{II}N_6]$ complexes, the influence of this global structural feature has been reported across the photocycle of numerous light-excited species (Figure 1). The photoinduced LS → HS transition

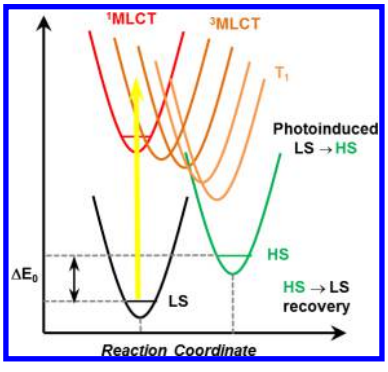

Figure 1. Schematic of the potential energy curves involved in the photoinduced LS → HS formation and the HS → LS recovery in d^6 complexes.

Received: November 23, 2014
Revised: December 23, 2014
Published: January 30, 2015

DOI: 10.1021/jp5117189
J. Phys. Chem. C 2015, 119, 3322−3330

proceeds from the ^{1}MLCT Franck−Condon state via intersystem crossing. The exact assignment of the mediating triplet manifold is currently a forefront topic in ultrafast optical[17−20] and X-ray sciences.[21−25] Complete active space second-order perturbation theory (CASPT2)[26−28] and density functional theory (DFT)[27,29] have been employed to predict the relative energy positions of the singlet, triplet, and quintet potential energy surfaces, along with their deactivating crossings. These calculations have shown that the energetic landscape is strongly affected by nonsymmetrical vibrational modes and overall geometrical distortions. Conversely, the kinetics of the HS → LS recovery often follow the "inverse energy gap law"[7,30] when the RC can be approximated by the isotropic change in average Fe−N bond length, ΔR_{av}. However, the rates of LS−HS interconversion are found to increase with the degree of distortion during SCO (e.g., from O_h to D_{3h} symmetry through the Bailar twist[31]), so that the high-frequency Fe−N stretching mode should be coupled to a low-frequency mode (e.g., torsional motion) in the effective RC.[32−35] Similarly, the unexpectedly long lifetimes manifested in several light-induced excited state trapping (LIESST) experiments have been ascribed to a multimodal RC that remains to be ascertained to date.[10,30,36]

Classifying and quantifying the geometrical distortions requires generalizing the stereochemical framework beyond the discrete space groups, by considering the polyhedral shape Q of the FCS as a continuous structural property.[37−42] Building a continuous shape measure (CShM) Φ_{S1} makes it possible to calibrate "how far" Q is from a polyhedron P of ideal shape S_1 in a definite symmetry point group (e.g., an octahedron). For quasi-octahedral complexes, this metric condenses the descriptors of molecular distortions given in terms of crystallographic parameters, such as $\zeta = \sum_{i=1}^{6}|R_i - R_{av}|$ where the R_i are the 6 M−L bond distances, or $\Sigma = \sum_{i=1}^{12}|90 - \phi_i|$, where the sum of the angular deviations from 90° for the 12 *cis* angles ϕ_i measures the departure from octahedricity.[15,16] Within the family of $[Fe^{II}N_6]$ complexes, the trends in CShM have revealed clear correlations between the geometry of their FCS and several of their observable physicochemical properties, e.g. chirality, SCO temperature, magnetic moment, or optical activity.[43] The present work demonstrates how this concept can be extended to the characterization of the FCS in transient photoexcited species. The structure adopted by the photoinduced HS state of solvated $[Fe(terpy)_2]^{2+}$(terpy: 2,2′:6′,2″-terpyridine) has been recently obtained with picosecond X-ray absorption spectroscopy (XAS). The excellent S/N ratio has allowed discriminating between the various predictions from DFT optimization in D_{2d} and D_2 symmetries. Based on these results, the changes in CShM between the LS and the transient HS states are extracted, providing novel insights into the multimodal RC for this benchmark molecule and other related photoactive Fe^{II} complexes.

MATERIALS AND METHODS

DFT Optimization. Density functional theory (DFT)[44,45] has been applied to the determination of the geometry adopted by the $[Fe(terpy)_2]^{2+}$ molecular complex in the singlet LS, the triplet, and the quintet HS state. The optimizations have been performed with the ADF program package[46] using the PBE[47] and RPBE[48] functionals, with the Slater-type TZP basis set of triple-ζ polarized quality from the ADF basis set database.[49,50] The calculations have been first conducted for the complex in the gas phase. The influence of the acetonitrile solvent has then been taken into account using the conductor-like screening model (COSMO).[51−54]

Evaluation of the Continuous Shape Measures. The continuous shape measures (CShM) with respect to two ideal polyhedrons chosen as the octahedron (OC-6) and the edge-bicapped tetrahedron (BCT-6) of D_{2d} symmetry have been evaluated using the program Shape 2.1.[37−42] These CShMs are employed to quantitatively describe the geometric distortions from a reference shape of ideal symmetry.

RESULTS AND DISCUSSION

From Continuous Shape Measures to Reaction Coordinates. When the conformation of a complex evolves from a shape S_1 to a shape S_2, several bond lengths R_i and bond angles β_j are concurrently modified. If none of the chemical bonds are broken, their variations are not independent from each other. In the structural parameter space $\{R_i, \beta_j\}$ spanned by the R_i and β_j, they are linked through an implicit multidimensional constraint function $\chi(R_i, \beta_j) = 0$, which exists insofar as the ligands retain their rigidity and their coordination to the metal. Taking the example of a chelate ring formed by a rigid bidentate ligand, the M−L bond distance R and the L−M−L bond angle β are related through $\sin(\beta/2) - d/2R = 0$, where d is the donor−donor distance (usually known as the bite angle). In order to establish the RC of the S_1−S_2 interconversion, it is necessary to elucidate the exact nature of $\chi(R_i, \beta_j) = 0$. The general structure−correlation principle postulates that the condition $\chi(R_i, \beta_j) = 0$ is maintained along the pathway of minimal energy in the structural parameter space $\{R_i, \beta_j\}$.[55,56] In other words, the geometries that can be physically adopted and observed experimentally are all satisfying $\chi(R_i, \beta_j) = 0$. In practice, this route can be probed by varying the crystallization conditions (e.g., solvents or counterions). Because of the differences in hydrogen bonding and packing forces, one of the equilibrium conformations energetically allowed that complies with $\chi(R_i, \beta_j) = 0$ is then adopted, so that, collectively, these static crystal structures can be envisaged as snapshots of the complex during the S_1−S_2 interconversion. With the extension of photocrystallography to the ultrafast regime,[57−59] it has become possible to infer $\chi(R_i, \beta_j) = 0$ from a direct tracking of transient structures. In many cases, $\chi(R_i, \beta_j) = 0$ can be expressed in terms of a few key structural parameters, thereby revealing the RC of the S_1−S_2 interconversion. For example, the structural changes between the LS and HS states of Fe^{II} complexes are predominantly observed in their FCS. Nevertheless, even with such a simplification, the description of their geometries cannot usually go beyond evidencing a global distortion from an ideal shape that belongs to a well-defined symmetry point group. It is therefore necessary to construct a generalized metric that enables treating the shape of a polyhedron as a continuously variable structural property. The continuous shape measure (ChM) Φ_{S1} is expressed as

$$\Phi_{S1} = \min\left(\frac{\sum_{k=1}^{N}|\overrightarrow{Q_k} - \overrightarrow{P_k}|^2}{\sum_{k=1}^{N}|\overrightarrow{Q_k} - \overrightarrow{Q_0}|^2}\right) \times 100$$

where the $\overrightarrow{Q_k}$ (k = 1, 2, ..., N) and $\overrightarrow{Q_0}$ are the position vectors of the N vertices and the center of mass for the polyhedron Q,[39,41,42] respectively. The $\overrightarrow{P_k}$ (k = 1, 2, ..., N) are the position vectors of the N vertices for the reference polyhedron P. A Φ_{S1}

DOI: 10.1021/jp5117189
J. Phys. Chem. C 2015, 119, 3322−3330

close to zero pinpoints that Q is a near ideal S_1. Given two reference polyhedra S_1 and S_2, Φ_{S1} lower than Φ_{S2} indicates that Q should be seen as a distorted S_1 rather than a distorted S_2. When the S_1-S_2 interconversion is followed in the two-dimensional map $\{\Phi_{S1}, \Phi_{S2}\}$ spanned by $\Phi_{S1}$and Φ_{S2}, the route of minimized energy identifies with the minimal distortion pathway $\Theta(\Phi_{S1}, \Phi_{S2}) = 0$,[39,41,42] which is unique and solely determined by the relative geometrical changes between S_1 and S_2. Consequently the RC can be made explicit as a function of polytopal rearrangement. The numerical evaluation of Φ_{S1} and Φ_{S2} requires access to the x, y, z coordinates of the atoms in the FCS, which are readily available from crystal structures. However, an alternative approach has to be devised for the systems that do not sustain long-range ordering. Accurate structural information about the FCS can be routinely extracted in any physical phase with X-ray absorption spectroscopy (XAS). Owing to the rapid optimization of optical pump−X-ray probe setups at storage ring and X-ray free electron laser facilities worldwide, the quality of the transient XAS spectra is now comparable to the one obtainable in static experiments, so that the FCS of short-lived solvated species is also within reach. The XAS analysis can be further used to discriminate between various predictions from DFT optimizations. Casting these results in terms of CShM allows visualizing the RC across the spin-state transition, as illustrated below for the particular case $[Fe(terpy)_2]^{2+}$ in solution.

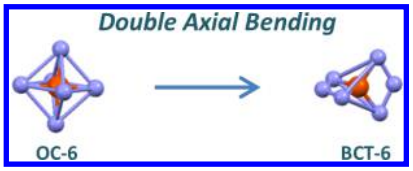

Figure 2. Schematic of the double axial bending converting an octahedron (OC-6) into an edge-bicapped tetrahedron (BCT-6) of D_{2d} symmetry.

As shown by single crystal X-ray diffraction, $[Fe(terpy)_2(ClO_4)_2.H_2O]$ displays a D_{2d} symmetry. The tridentate coordination is accompanied by a preferential π back-bonding, which renders $Fe-N_{Axial}$ (1.89 Å) significantly shorter than $Fe-N_{Distal}$ (1.98 Å). For the solvated complex, the XAS analysis of the FCS concurs with these values, while the XANES fingerprints indicate that the complex nevertheless retains a quasi-O_h symmetry. Recently, picosecond XAS spectroscopy has been employed to study the structure of the photoinduced HS state. The anisotropic distortion of the FCS has been captured through the detection of distinct ΔR for the two nonequivalent Fe−N bonds. Comparison with DFT optimization demonstrates that the structure of the photoinduced HS state can be viewed equally well as the ^5E state in D_{2d} geometry or as the average ^5B structure that originates from a dynamic Jahn−Teller effect in the D_2 geometry (see previous article). Without bond breaking, an octahedron (OC-6) can only be deformed into an edge-bicapped tetrahedron (BCT-6) of D_{2d} symmetry via a double axial bending, as shown in Figure 2.

The minimal distortion pathway $\Theta(\Phi_{OC\text{-}6}, \Phi_{BCT\text{-}6}) = 0$ between these two reference polyhedra is unique and solely determined by the correlated geometrical changes imposed by the interconversion.[42] Its analytical expression (from eq 11 of ref 42) is automatically returned by the program Shape 2.1.[39,41] For the HS state of solvated $[Fe(terpy)_2]^{2+}$, the distortion can be traced back to the longer Fe−N bond distances and the smaller bite angles subtended by the rigid tridentate ligand. The ChSM with respect to $\Phi_{OC\text{-}6}$ and $\Phi_{BCT\text{-}6}$ are evaluated from the DFT coordinates and displayed in the CShM map $\{\Phi_{OC\text{-}6}, \Phi_{BCT\text{-}6}\}$, for the LS and the various HS states in D_{2d} and D_2 symmetry obtained with the RPBE (Figure 3a) and the PBE (Figure 3b) functionals (see previous article). The route $\Theta(\Phi_{OC\text{-}6}, \Phi_{BCT\text{-}6}) = 0$ is indicated by the solid purple line in both figures. Clearly, the LS and HS states interconvert through a double axial bending, thereby identifying the RC that drives the spin-state transition. This RC consists of concerted changes in specific bond lengths and bond angles. Considering the dynamic Jahn−Teller effect in the degenerate ^5E manifold that yields the average ^5B-D_2 state is crucial for reaching consistency between the experimental and theoretical descriptions of the electronic and geometric structures adopted by the HS state of solvated $[Fe(terpy)_2]^{2+}$(see previous article). The fact that $\Phi_{OC\text{-}6}$ (^5E-D_{2d}) ~ $\Phi_{OC\text{-}6}$ (^5B-D_2) and $\Phi_{BCT\text{-}6}$ (^5E-D_{2d}) ~ $\Phi_{BCT\text{-}6}$ (^5B-D_2) nevertheless shows that, using these generalized metrics, the anisotropic distortions in the FCS of these two states are very similar. It should be noted that the $^5B_2$ state in D_{2d} symmetry also falls on this double axial bending route, although further along as it presents larger deviation from O_h symmetry than any of the other states.

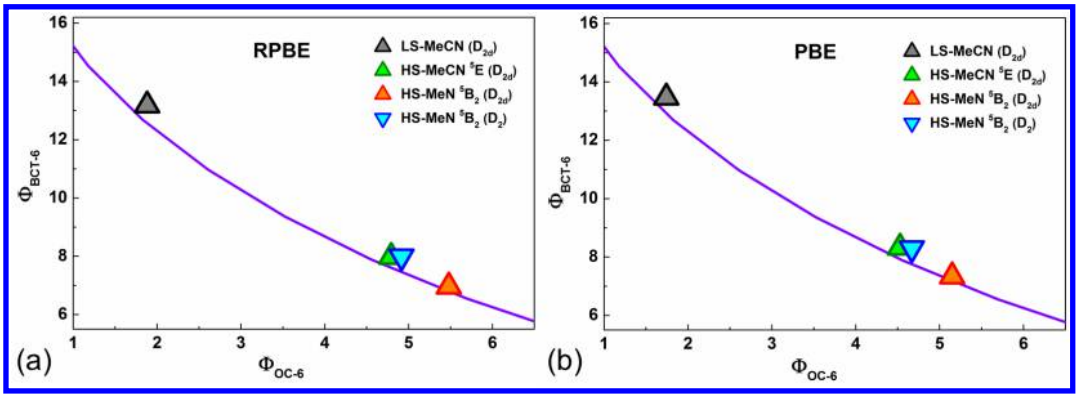

Figure 3. CShM map for the LS-HS interconversion of solvated $[Fe(terpy)_2]^{2+}$ constructed from (a) the RPBE structures and (b) the PBE structures (this work). The continuous line represents the minimal distortion path between the octahedron and the edge-bicapped tetrahedron.

DOI: 10.1021/jp5117189
J. Phys. Chem. C 2015, 119, 3322−3330

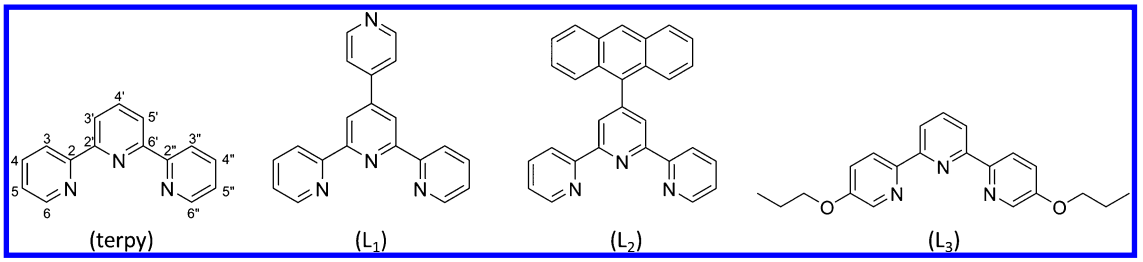

Figure 4. Schematic of the substituted terpy ligands that yield complexes with a LS ground state.

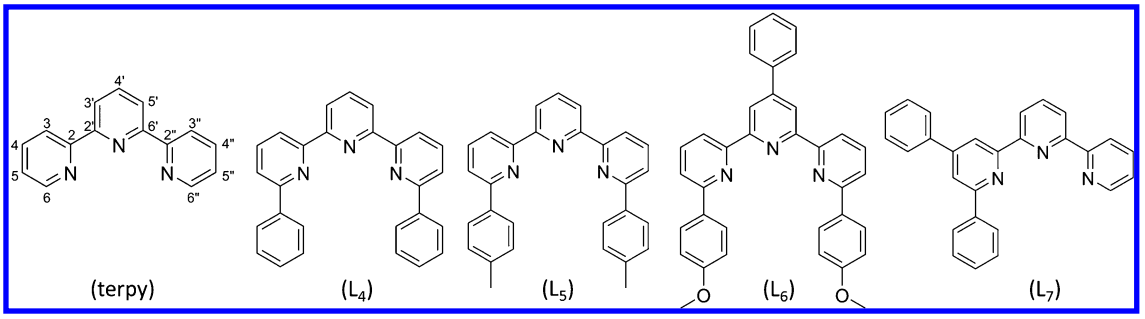

Figure 5. Schematic of the substituted terpy ligands that yield complexes with a HS ground state.

Quantifying Chemical and Solid-State Effects in Fe^{II} Complexes of Terpy Derivatives. An expanding research area in the synthetic chemistry of SCO complexes focuses on understanding how first-shell and second-shell interactions can tune the strength of the ligand field (LF) around the crossover point. The incorporation of steric bulk and steric strain in the ligand scaffold has long been known to have a direct impact on the average M−L bond length. The associated hindrance usually causes an overall elongation ΔR_{av}, which weakens the LF and favors the thermal population of the HS state. However, the rationalization of the finer trends observed between the nature of the chemical substitution, the structural anisotropy of the FCS, and the spin-state of a complex is still largely empirical. The identification of the RC for the LS−HS interconversion in solvated $[Fe(terpy)_2]^{2+}$ as a double axial bending provides a benchmark to analyze in greater details the relationship between substitution, distortion, and spin state for the family Fe^{II} complexes built on terpy derivatives. The introduction of substituents at the 4′-position, e.g., 4′-(4‴-pyridyl)-2,2′:6′,2″-terpyridine (L_1)[60] or 4′-(9-anthryl)-2,2′:6′,2″-terpyridine (L_2),[61] or at the 5- and 5′-positions, e.g., 5,5″-bis(propoxy)-2,2′:6′,2″-terpyridine (L_3),[62] produces complexes with a LS ground state (see Figure 4). On the other hand, substitutions at the 6- and 6″-positions yield complexes with a HS ground state, as for e.g. 6,6″-diphenyl-2,2′:6′,2″-terpyridine (L_4),[63] 6,6″-di(*p*-toly)-2,2′:6′,6″-terpyridine (L_5),[64] or 6,6″-bis(5′-methoxyphenyl)-4′-phenyl-2,2′:6′,2″-terpyridine (L_6)[65] (Figure 5). For all these complexes, the weak LF has been tentatively ascribed to the face-to-face π stacking between the phenyl or aryl substituent rings and the pyridyl ring of the two opposite *mer*-tridentate ligands. This intramolecular interaction induces a significant deviation from planarity in the terpy scaffold, hence some structural anisotropy in the FCS, although the rings themselves remain planar. The respective $\Phi_{OC\text{-}6}$ and $\Phi_{BCT\text{-}6}$ are evaluated using the *x*, *y*, *z* coordinates from the reported crystal structures. As expected, they do not fall on the double axial bending RC in $\{\Phi_{OC\text{-}6}, \Phi_{BCT\text{-}6}\}$ in Figure 6. However, it can be concluded that, despite the differences observed in the bond lengths and bond angles of their FCS, the anisotropic distortions with respect to $\Phi_{OC\text{-}6}$ and $\Phi_{BCT\text{-}6}$ are quantitatively equivalent. The comparison with the CShM obtained for the HS state of solvated $[Fe(terpy)_2]^{2+}$ also highlights the fact that chemically stabilized HS states do not necessarily constitute accurate structural equivalent of the photoinduced HS state for the complex with unsubstituted ligands.

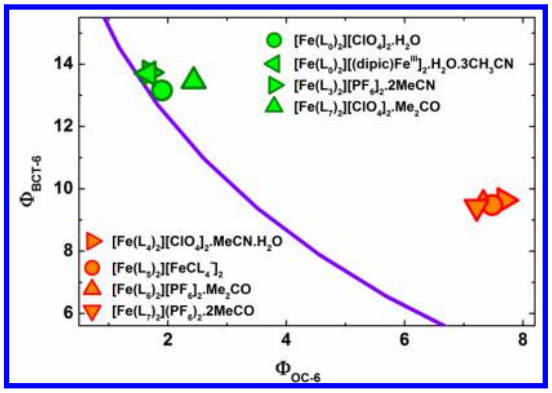

Figure 6. CShM map for the reported crystal structures of Fe^{II} complexes incorporating terpy, L_3, L_4, L_5, L_6, and L_7 shown in Figures 4 and 5.

In the crystalline phase, the spin state of Fe^{II} complexes can be further influenced by second-shell interactions involving solvent molecules or counterions and by packing forces. The reported crystals of $[Fe(terpy)_2][X_2]$ demonstrate a LS complex (e.g., $[Fe(terpy)_2][ClO_4]_2{\cdot}H_2O$[66] or $[Fe(terpy)_2][(dipic)_2Fe^{III}]_2{\cdot}H_2O{\cdot}3CH_3CN$[67] where dipic = $C_7H_3NO_4$) regardless of the nature of the counterion X.[66−68] However, with 4,6-diphenyl-2,2′:6′,2″-terpyridine (L_7), $[Fe(L_7)_2][ClO_4]_2{\cdot}2MeCO$ is a LS complex, while $[Fe(L_7)_2][PF_6]_2{\cdot}2MeCO$ is a HS complex.[63] Determining the interaction responsible for the weaker LF is not straightforward: no intramolecular π stacking is observed, but the O atom of the acetone molecule promotes some degree of hydrogen bonding within the lattice. Nevertheless, the overall distortion of $[Fe(L_7)_2][PF_6]_2{\cdot}2MeCO$ measured with $\Phi_{OC\text{-}6}$ and $\Phi_{BCT\text{-}6}$ is

DOI: 10.1021/jp5117189
J. Phys. Chem. C 2015, 119, 3322−3330

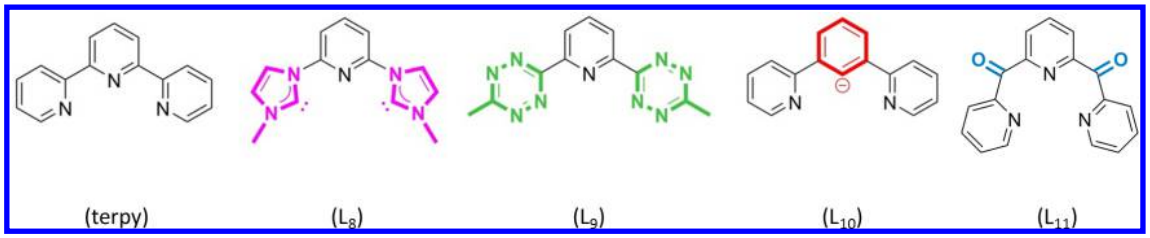

Figure 7. Schematic of recently synthesized tridentate ligands discussed in the main text.

comparable to the one presented by the chemically stabilized HS complexes.

Toward Tailoring the Metal-Centered Manifolds of Tridentate Fe^{II} Complexes. It is well established that the photoinduced functionality of transition metal complexes is largely governed by the nature of the lowest thermally equilibrated excited (thexi) state.[69,70] For instance, the long lifetimes (~microseconds range) displayed by the metal-to-ligand charge transfer (MLCT) states in compounds of 4d (e.g., Ru) and 5d (e.g., Os, Ir) elements promote their participation to endoenergetic reactions. The population of metastable metal centered (MC) states at room temperature in compounds of 3d (e.g., Fe) elements imparts electronic and magnetic bistability with practical applications. The properties of the thexi state itself depend in turn upon the manifold of high-lying excited states. In particular, the lifetime of the ^{3}MLCT in several Ru complexes can be significantly extended through the destabilization of the ^{3}MC state, which is otherwise thermally accessible. This is generally achieved by employing ligands with (1) electron accepting/donating substituents, (2) large conjugated π-systems,[71,72] or (3) strong σ-donor capabilities.[73−75] Adapting successfully these strategies to molecular systems based on low-Z elements would allow developing nontoxic and cost-effective sensitizers[76−78] or even emitters. Because of the intrinsically lower ligand field splitting in Fe as compared to Ru, only (3) has resulted so far into a demonstrated increase of the ^{3}MLCT lifetime for an Fe^{II} compound, namely $[Fe(L_8)_2]^{2+}$ (where L_8 = 2,6-bis(3-methylimidazole-1-ylidine)pyridine)[79] shown in Figure 7. This complex incorporates a novel N-heterocyclic carbene ligand in a *mer*-tridentate coordination analogous to that of $[Fe(terpy)_2]^{2+}$.[79] Femtosecond transient optical absorption spectroscopy has established the unprecedented 9 ps lifetime of its ^{3}MLCT in MeCN, which is about 60 times longer than the 145 fs displayed by $[Fe(terpy)_2]^{2+}$.[79] These measurements have also evidenced that the HS ^{5}MC state is not populated.[79] This complex solvated in MeCN has been investigated numerically with DFT and time-dependent DFT techniques.[80] Taking the average Fe−C bond lengths q_{C1} and q_{C2} of the two ligands as structural variables, the multidimensional search across the parameter space $\{q_{C1}, q_{C2}\}$ has unveiled the electronic and geometric structures of the LS ground state (GS) and of the excited states ^{3}MLCT, ^{3}MC, and HS ^{5}MC. These calculations have unambiguously revealed that the ^{3}MC and HS ^{5}MC states are destabilized with respect to the ^{3}MLCT state. The atomic rearrangements in the ^{3}MC state are primarily localized on a single ligand, where q_{C1} undergoes an elongation of 0.13 Å, while the Fe−N bond q_{N1} increases by 0.28 Å. On the second ligand, q_{C2} remains unchanged, while q_{N2} only increases by about 0.13 Å. In the HS ^{5}MC state, q_{C1} and q_{C2} become equal with an overall expansion of 0.25 Å, while the bond elongation reaches 0.33 Å for q_{N1} and q_{N2}. The computational optimization has also uncovered a low-energy transition path between ^{3}MLCT and ^{3}MC, with a subsequent crossing back to the LS GS. Analyzing the distortions of the excited states in terms of CShM offers complementary insights into the structural dynamics triggered by photoabsorption. The $\Phi_{OC\text{-}6}$ and $\Phi_{BCT\text{-}6}$ for the LS GS, ^{3}MLCT, ^{3}MC, and HS ^{5}MC are displayed in $\{\Phi_{OC\text{-}6}, \Phi_{BCT\text{-}6}\}$ as shown in Figure 8a. First, the complex retains a noticeable D_{2d} symmetry regardless of the spin multiplicity. It should be reemphasized here that the numerical search across $\{q_{C1}, q_{C2}\}$ was performed without geometry constraint.[80] Second, along the double axial bending RC, which also spans the path of minimized energy, the ^{3}MC is encountered before the HS ^{5}MC, which is then "more" distorted when the $\Phi_{OC\text{-}6}$ and $\Phi_{BCT\text{-}6}$ CShM are considered as generalized metrics. This finding readily explains the deactivation of the ^{3}MLCT by the ^{3}MC state and the absence of population of the HS ^{5}MC reported in the theoretical study.[80] The low-energy transition path between the ^{3}MLCT and the ^{3}MC is related to the fact that the ^{3}MC possess a geometry that is accommodating the intrinsic symmetry of the ligand without further distortion. By comparison, a similar graph for $[Fe(terpy)_2]^{2+}$ (Figure 8b) clearly shows that the LS → ^{3}MC transition does not follow a double axial bending and that, along this path of minimal energy, the HS ^{5}MC is formed instead. Using the angular overlap model,[81] quantitative estimates for the rates of singlet−triplet and triplet−quintet intersystem crossing can be obtained as a function of the OC-6 to BCT-6 deformation through double axial bending. Activation energy barriers can also be evaluated as a function of this RC with DFT, CASPT2, or empirical ligand field molecular mechanic.[82] Such calculations for both molecules are currently underway. In addition, the contrasting behavior of the two ligands in the ^{3}MC state raises fundamental issues about the detailed mechanism of the ultrafast intramolecular ET process at the very early times, after population of the ^{1}MLCT Franck−Condon state. For example, what is the extent of charge localization on one of the ligands in the ^{3}MLCT (if any) before it gets preferentially distorted in the ^{3}MC? Answering such questions will require complementing the spectroscopic and structural characterization with spin-state information through studies enabled by X-ray free electron facilities.[25] Femtosecond resonant inelastic scattering could be particularly well-suited to track the real-time evolution of the covalency in the Fe−C bond.[83]

A distinct strength of the CShM approach is that it solely requires the optimization of a few key structures in terms of a single structural parameter, i.e., the RC of the LS−HS interconversion. This method should assist a rapid screening by computational means of promising molecular architectures. For example, the CShM maps for the Fe^{II} complexes based on the related pincer ligands, such as $[Fe(L_9)_2]^{2+}$ (where L_9 = bis(tetrazinylpyridine))[84] and $[Fe(L_{10})_2]$ (where L_{10} = bis-

DOI: 10.1021/jp5117189
J. Phys. Chem. C 2015, 119, 3322−3330

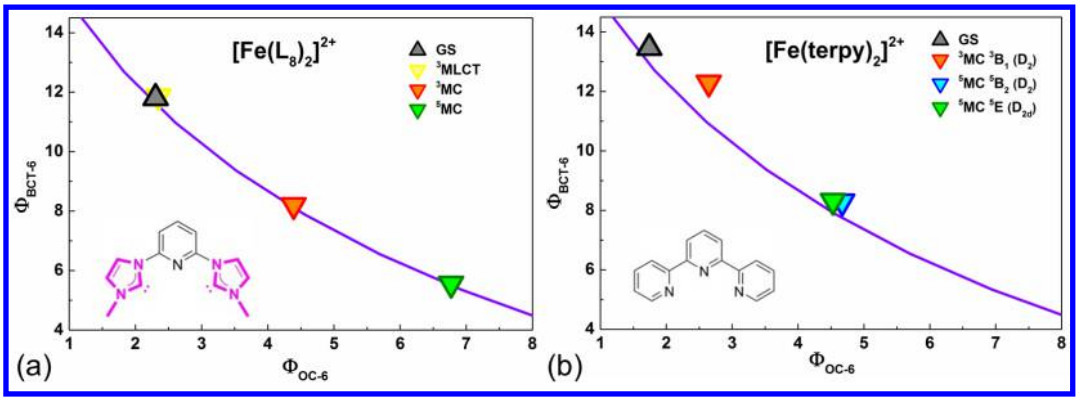

Figure 8. CShM map for (a) $[Fe(L_8)_2]^{2+}$ optimized with PBE0/6-311G(d, p)/PCM(MeCN)[81] and (b) $[Fe(terpy)_2]^{2+}$ optimized with PBE in MeCN (this work). The continuous line represents the minimal distortion path between the octahedron and the edge-bicapped tetrahedron.

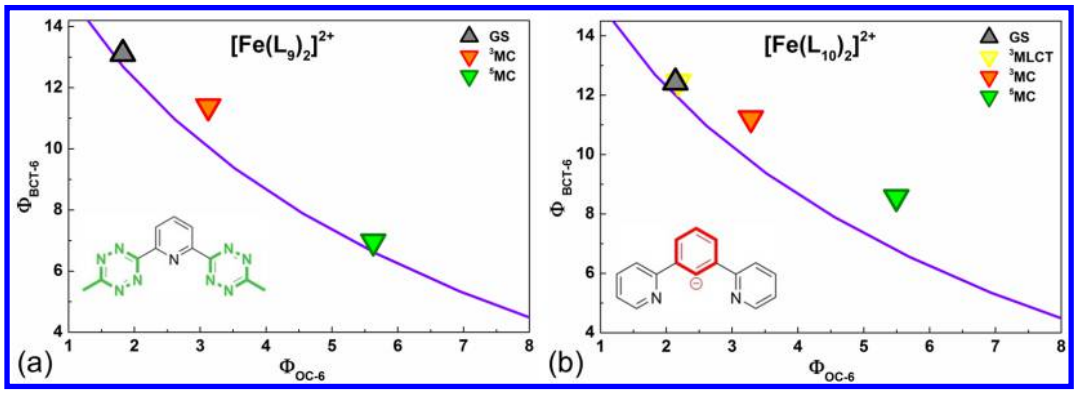

Figure 9. CShM maps for (a) $[Fe(L_9)_2]^{2+}$ optimized with B3LYP/LANL2DZ/6-31G(d,p)[85] (b) $[Fe(L_{10})_2]^{2+}$optimized with B3LYP.[86] The continuous line represents the minimal distortion path between the octahedron and the edge-bicapped tetrahedron.

(dipyridylbenzene))[85] in Figure 7 can be constructed from the published DFT structures (Figures 9a and 9b). This allows inferring that the photophysics of both complexes should be very similar to $[Fe(terpy)_2]^{2+}$, with the possibility of very fast ground state recovery or decomplexation in the case of $[Fe(L10)_2]^{2+}$. Further derivatization of these ligands may nevertheless produce improved complexes, especially for $[Fe(L_9)_2]^{2+}$ since the $\Phi_{OC\text{-}6}$ and $\Phi_{BCT\text{-}6}$ are close to the ones of $[Fe(L_{10})_2]^{2+}$.

Finally, the last known design strategy introduced for extending the lifetime of *mer*-tridentate Ru based complexes should be considered. It utilizes the destabilization of the ^{3}MC levels through enforcing a near ideal O_h geometry for the FCS, hence maximizing the ligand field splitting. Such a geometry is obtained by opening the bite angle in the *mer*-tridentate coordination.[86,87] The viability of this approach for Fe has been demonstrated with the recent synthesis of $[Fe(L_{11})_2]^{2+}$ (where L_{11} = 2,6-bis(2-carboxypyridyl)pyridine), shown in Figure 7).[88] In this compound, the ^{3}MC might be energetically stabilized over the HS ^{5}MC state.[88] Figure 10 shows the $\Phi_{OC\text{-}6}$ and the $\Phi_{BCT\text{-}6}$ for $[Fe(L_{11})_2]^{2+}$ obtained from the reported crystal structure.[88]

As expected from the quasi-O_h geometry, the $\Phi_{OC\text{-}6}$ is very close to 0. The comparison with $[Fe(terpy)_2]^{2+}$ displayed in the same graph indicates that chemical substitutions should allow sampling quite different regions of the CShM map, where the departure from O_h symmetry might be minimized.

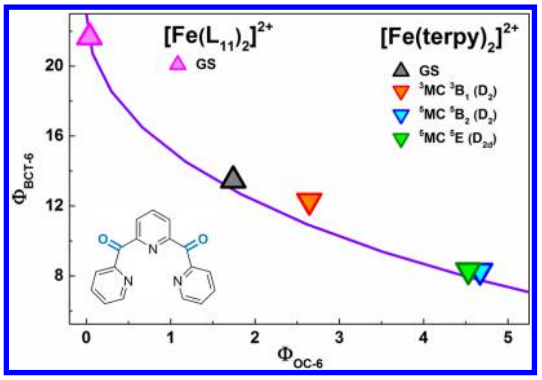

Figure 10. CShM maps for $Fe(L_{11})_2]^2$ (from crystallographic structure) and $[Fe(terpy)_2]^{2+}$ from the DFT optimization with PBE, for comparison. The continuous line represents the minimal distortion path between the octahedron and the edge-bicapped tetrahedron.

CONCLUSIONS

Using picosecond X-ray absorption spectroscopy and DFT optimizations, the photoinduced HS state of solvated $[Fe(terpy)_2]^{2+}$ has been recently assigned as the average ^{5}B-D_2 structure caused by the dynamic Jahn−Teller effect in the degenerate ^{5}E-D_{2d} manifold. Based on these results, the CShM $\Phi_{OC\text{-}6}$ and $\Phi_{BCT\text{-}6}$ have been employed to quantify the anisotropic deformation of the first coordination sphere for this short-lived state. The minimal distortion pathway, which reveals the RC of the LS−HS interconversion, has been

DOI: 10.1021/jp5117189
J. Phys. Chem. C 2015, 119, 3322−3330

established as a double axial bending. This study clearly demonstrates that the CShM formalism can be extended to the structural characterization of transient excited states in real time. The methodology complements ultrafast photocrystallography, which cannot be applied to samples that do not present any long-range order or when the crystallization process strongly affects the conformations and the dynamics through hydrogen bonding or crystal packing. Following the identification of the RC in solution, the CShM $\Phi_{OC\text{-}6}$ and $\Phi_{BCT\text{-}6}$ for various complexes incorporating substituted terpy ligands have been evaluated. These generalized metrics can delineate trends in the combined influence of first-shell and second-shell interactions on the spin state observed in the crystalline phase. Overall, the RC that emerges from the minimal distortion pathway can bridge the description of the structural changes that take place in Fe^{II} complexes, from the solution to the solid phase. In particular, accessing the CShM of the photoinduced and the thermally induced HS state for a given SCO complex should pinpoint structural similarities or differences, the distinction being often essential to the optimization of the LIESST phenomenon[89−91] toward specific applications.

For a recently reported Fe^{II} complex, which displays an unprecedentedly long ^{3}MLCT lifetime, the CShM $\Phi_{OC\text{-}6}$ and $\Phi_{BCT\text{-}6}$ of the singlet, triplet, and quintet states have been extracted from the predicted DFT structures. Comparison with $[Fe(terpy)_2]^{2+}$ explains the contrasting deactivation mechanisms. The possibility to infer this key aspect of the photophysics from a few DFT structures should offer distinct perspectives for systematically and rapidly screening novel molecular architectures by computational methods. In particular, the methodology could deliver valuable diagnostics about the excited-state manifold of Cu(I) complexes, which have been found to be efficient sensitizers,[92] or the one of Cu(II) complexes, for which the photoinduced structural dynamics are highly complicated by the Jahn−Teller effect.[14] Such investigations will likely contribute to the development of molecular design strategies aiming at tailoring the properties of metal-centered states, which have largely been considered detrimental so far for photoreactivity. As a unifying concept in stereochemistry, mapping the ultrafast variations in CShM across the mesoscale will also participate to the elaboration of innovative SCO materials with synergetic functionalities based on polymorphism.

AUTHOR INFORMATION

Corresponding Author

*E-mail sophie.canton@maxlab.lu.se (S.E.C.).

Notes

The authors declare no competing financial interest.

ACKNOWLEDGMENTS

The Swedish Research Council and the Crafoord Foundation are greatly acknowledged as funding sources. X.Z. was supported by the U.S. Department of Energy, Office of Science, Office of Basic Energy Sciences, under Contract DE-AC02-06CH11357. This work was supported by allocations of computing time from the Swiss National Supercomputing Centre (CSCS) under Project IDs s103 and s296 and the Center for Advanced Modeling Science (CADMOS) under Project ID CTESIM. The authors also thank financial support from the Spanish Ministerio de Economía y Competitividad (Project CTQ2011-23862-C02-02) and Generalitat de Catalunya (Project 2009SGR-1459). We thank Andreas Hauser for helpful comments and stimulating discussions. Dr L. Fredin and Pr P. Persson are also gratefully acknowledged for very useful discussions.

REFERENCES

(1) Baadji, N.; Piacenza, M.; Tugsuz, T.; Della Sala, F.; Maruccio, G.; Sanvito, S. Electrostatic Spin Crossover Effect in Polar Magnetic Molecules. *Nat. Mater.* **2009**, *8*, 813−817.

(2) Feng, X.; Mathonière, C.; Jeon, I.-R.; Rouzières, M.; Ozarowski, A.; Aubrey, M. L.; Gonzalez, M. I.; Clérac, R.; Long, J. R. Tristability in a Light-Actuated Single-Molecule Magnet. *J. Am. Chem. Soc.* **2013**, *135*, 15880−15884.

(3) Gaspar, A. B.; Seredyuk, M. Spin Crossover in Soft Matter. *Coord. Chem. Rev.* **2014**, *268*, 41−58.

(4) Létard, J.-F.; Guinneau, P.; Goux-Capes, L. Towards Spin Crossover Applications. *Top. Curr. Chem.* **2004**, *235*, 221−249.

(5) Ohkoshi, S.-i.; Imoto, K.; Tsunobuchi, Y.; Takano, S.; Tokoro, H. Light-Induced Spin-Crossover Magnet. *Nat. Chem.* **2011**, *3*, 564−669.

(6) Roubeau, O.; Colin, A.; Schmitt, V.; Clérac, R. Thermoreversible Gels as Magneto-Optical Switches. *Angew. Chem., Int. Ed.* **2004**, *43*, 3283−3286.

(7) Buhks, E.; Navon, G.; Bixon, M.; Jortner, J. Spin Conversion Processes in Solutions. *J. Am. Chem. Soc.* **1980**, *102*, 2918−2923.

(8) Bernien, M.; Wiedemann, D.; Hermanns, C. F.; Krueger, A.; Rolf, D.; Kroener, W.; Mueller, P.; Grohmann, A.; Kuch, W. Spin Crossover in a Vacuum-Deposited Submonolayer of a Molecular Iron(II) Complex. *J. Phys. Chem. Lett.* **2012**, *3*, 3431−3434.

(9) Hauser, A. Ligand Field Theoretical Considerations. *Top. Curr. Chem.* **2004**, *233*, 49−58.

(10) Schenker, S.; Stein, P. C.; Wolny, J. A.; Brady, C.; McGarvey, J. J.; Toftlund, H.; Hauser, A. Biphasic Behavior of the High-Spin → Low-Spin Relaxation of $[Fe(btpa)](PF_6)_2$ in Solution (btpa = N,N,N′,N′-Tetrakis(2-pyridylmethyl)-6,6′-bis(aminomethyl)-2,2′-bipyridine). *Inorg. Chem.* **2000**, *40*, 134−139.

(11) Zhou, J.; Wang, Q.; Sun, Q.; Kawazoe, Y.; Jena, P. J. Strain-Induced Spin Crossover in Phthalocyanine-Based Organometallic Sheets. *Phys. Chem. Lett.* **2012**, *3*, 3109−3114.

(12) Bowman, D. N.; Jakubikova, E. Low-Spin versus High-Spin Ground State in Pseudo-Octahedral Iron Complexes. *Inorg. Chem.* **2012**, *51*, 6011−6019.

(13) Halcrow, M. A. Structure:Function Relationships in Molecular Spin-Crossover Complexes. *Chem. Soc. Rev.* **2011**, *40*, 4119−4142.

(14) Halcrow, M. A. Jahn-Teller Distortions in Transition Metal Compounds, and their Importance in Functional Molecular and Inorganic Materials. *Chem. Soc. Rev.* **2013**, *42*, 1784−1795.

(15) Marchivie, M.; Guionneau, P.; Létard, J.-P.; Chasseau, D. Towards Direct Correlations Between Spin-Crossover and Structural Features in Iron(II) Complexes. *Acta Crystallogr., Sect. B: Struct. Sci.* **2003**, *59*, 479−486.

(16) Marchivie, M.; Guionneau, P.; Létard, J.-F.; Chasseau, D. Photoinduced Spin-Transitions: the Role of the Iron(II) Environment Distortion. *Acta Crystallogr., Sect. B: Struct. Sci.* **2005**, *61*, 25−28.

(17) Bertoni, R.; Lorenc, M.; Tissot, A.; Servol, M.; Boillot, M. L.; Collet, E. Femtosecond Spin-State Photoswitching of Molecular Nanocrystals Evidenced by Optical Spectroscopy. *Angew. Chem., Int. Ed.* **2012**, *51*, 7485−7489.

(18) Consani, C.; Prémont-Schwarz, M.; ElNahhas, A.; Bressler, C.; van Mourik, F.; Cannizzo, A.; Chergui, M. Vibrational Coherences and Relaxation in the High-Spin State of Aqueous $[Fe^{II}(bpy)_3]^{2+}$. *Angew. Chem.* **2009**, *121*, 7320−7323.

(19) Marino, A.; Chakraborty, P.; Servol, M.; Lorenc, M.; Collet, E.; Hauser, A. The Role of Ligand-Field States in the Ultrafast Photophysical Cycle of the Prototypical Iron(II) Spin-Crossover Compound $[Fe(ptz)_6](BF_4)_2$. *Angew. Chem., Int. Ed.* **2014**, *53*, 3863−3867.

DOI: 10.1021/jp5117189
J. Phys. Chem. C 2015, 119, 3322−3330

(20) Smeigh, A. L.; Creelman, M.; Mathies, R. A.; McCusker, J. K. Femtosecond Time-Resolved Optical and Raman Spectroscopy of Photoinduced Spin Crossover: Temporal Resolution of Low-to-High Spin Optical Switching. *J. Am. Chem. Soc.* **2008**, *130*, 14105−14117.
(21) Bressler, C.; Milne, C.; Pham, V.-T.; ElNahhas, A.; van der Veen, R. M.; Gawelda, W.; Johnson, S.; Beaud, P.; Grolimund, D.; Kaiser, M.; et al. Femtosecond XANES Study of the Light-Induced Spin Crossover Dynamics in an Iron(II) Complex. *Science* **2009**, *323*, 489−492.
(22) Chergui, M. Ultrafast Studies of the Light-Induced Spin Change in Fe(II)-Polypyridine Complexes. In *Spin-Crossover Materials: Properties and Applications*; Halcrow, M. A., Ed.; John Wiley & Sons Ltd.: Oxford, UK, 2013; doi 10.1002/9781118519301.ch15.
(23) Lemke, H. T.; Bressler, C.; Chen, L. X.; Fritz, D. M.; Gaffney, K. J.; Galler, A.; Gawelda, W.; Haldrup, K.; Hartsock, R. W.; Ihee; Kim, J.; et al. Femtosecond X-ray Absorption Spectroscopy at a Hard X-ray Free Electron Laser: Application to Spin Crossover Dynamics. *J. Chem. Phys. B* **2013**, *117*, 735−740.
(24) McCusker, J. K. X-ray Spectroscopy: Enlightened State. *Nat. Phys.* **2014**, *10*, 476−477.
(25) Zhang, W.; Alonso-Mori, R.; Bergmann, U.; Bressler, C.; Chollet, M.; Galler, A.; Gawelda, W.; Hadt, R. G.; Hartsock, R. W.; Kroll, T.; et al. Tracking Excited-State Charge and Spin Dynamics in Iron Coordination Complexes. *Nature* **2014**, *509*, 345−348.
(26) Graaf, C. D.; Sousa, C. On the Role of the Metal-to-Ligand Charge Transfer States in the Light-Induced Spin Crossover in $Fe^{II}(bpy)_3$. *Int. J. Quantum Chem.* **2011**, *111*, 3385−3393.
(27) Papai, M.; Vanko, G.; de Graaf, C.; Rozgonyi, T. Theoretical Investigation of the Electronic Structure of Fe(II) Complexes at Spin-State Transitions. *J. Chem. Theory Comput.* **2013**, *9*, 509−519.
(28) Sousa, C.; de Graaf, C.; Rudavskyi, A.; Broer, R.; Tatchen, J.; Etinski, M.; Marian, C. M. Ultrafast Deactivation Mechanism of the Excited Singlet in the Light-Induced Spin Crossover of $[Fe(2,2'\text{-bipyridine})_3]^{2+}$. *Chem.—Eur. J.* **2013**, *19*, 17541−17551.
(29) Suaud, N.; Bonnet, M.-L.; Boilleau, C.; Labèguerie, P.; Guihéry, N. Light-Induced Excited Spin State Trapping: Ab Initio Study of the Physics at the Molecular Level. *J. Am. Chem. Soc.* **2008**, *131*, 715−722.
(30) Hauser, A.; Enachescu, C.; Lawson-Daku, M. L.; Vargas, A.; Amstutz, N. Low-Temperature Lifetimes of Metastable High-Spin States in Spin-Crossover and in Low-Spin Iron(II) Compounds: The Rule and Exceptions to the Rule. *Coord. Chem. Rev.* **2006**, *250*, 1642−1652.
(31) Bailar, J. C., Jr. Some Problems in the Stereochemistry of Coordination Compounds: Introductory Lecture. *J. Inorg. Nucl. Chem.* **1958**, *8*, 165−175.
(32) Chang, H. R.; McCusker, J. K.; Toftlund, H.; Wilson, S. R.; Trautwein, A. X.; Winkler, H.; Hendrickson, D. N. [Tetrakis(2-pyridylmethyl)ethylenediamine]iron(II) Perchlorate, the First Rapidly Interconverting Ferrous Spin-Crossover Complex. *J. Am. Chem. Soc.* **1990**, *112*, 6814−6827.
(33) McCusker, J. K.; Rheingold, A. L.; Hendrickson, D. N. Variable-Temperature Studies of Laser-Initiated $^5T_2 \rightarrow {}^1A_1$ Intersystem Crossing in Spin-Crossover Complexes: Empirical Correlations between Activation Parameters and Ligand Structure in a Series of Polypyridyl Ferrous Complexes. *Inorg. Chem.* **1996**, *35*, 2100−2112.
(34) McCusker, J. K.; Walda, K. N.; Dunn, R. C.; Simon, J. D.; Magde, D.; Hendrickson, D. N. Sub-picosecond $\Delta S = 2$ Intersystem Crossing in Low-Spin Ferrous Complexes. *J. Am. Chem. Soc.* **1992**, *114*, 6919−6920.
(35) McCusker, J. K.; Walda, K. N.; Dunn, R. C.; Simon, J. D.; Magde, D.; Hendrickson, D. N. Subpicosecond $^1MLCT \rightarrow {}^5T_2$ Intersystem Crossing of Low-Spin Polypyridyl Ferrous Complexes. *J. Am. Chem. Soc.* **1993**, *115*, 298−307.
(36) Buron-Le Cointe, M.; Hébert, J.; Baldé, C.; Moisan, N.; Toupet, L.; Guionneau, P.; Létard, J. F.; Freysz, E.; Cailleau, H.; Collet, E. Intermolecular Control of Thermoswitching and Photoswitching Phenomena in Two Spin-Crossover Polymorphs. *Phys. Rev. B* **2012**, *85*, 064114.
(37) Alvarez, S.; Alemany, P.; Casanova, D.; Cirera, J.; Llunell, M.; Avnir, D. Shape Maps and Polyhedral Interconversion Paths in Transition Metal Chemistry. *Coord. Chem. Rev.* **2005**, *249*, 1693−1708.
(38) Alvarez, S.; Avnir, D.; Llunell, M.; Pinsky, M. Continuous Symmetry Maps and Shape Classification. The Case of Six-Coordinated Metal Compounds. *New J. Chem.* **2002**, *26*, 996−1009.
(39) Alvarez, S.; Ruiz, E. Self-Assembly of Coordination Compounds: Design Principles. In *Supramolecular Chemistry, From Molecules to Nanomaterials*; Steed, J. W., Gale, P. A., Eds.; John Wiley & Sons: Chichester, UK, 2012; Vol. 5, pp 1993−2044; ISBN 978-0-470-74640-0.
(40) Dollase, W. A Method of Determining the Distortion of Coordination Polyhedral. *Acta Crystallogr., Sect. A* **1974**, *30*, 513−517.
(41) Pinsky, M.; Avnir, D. Continuous Symmetry Measures. 5. The Classical Polyhedra. *Inorg. Chem.* **1998**, *37*, 5575−5582.
(42) Casanova, D.; Cirera, J.; Llunell, M.; Alemany, P.; Avnir, D.; Alvarez, S. Minimal Distortion Pathways in Polyhedral Rearrangements. *J. Am. Chem. Soc.* **2004**, *126*, 1755−1763.
(43) Alvarez, S. Relationships Between Temperature, Magnetic Moment and Continuous Symmetry Measures in Spin Crossover Complexes. *J. Am. Chem. Soc.* **2003**, *125*, 6795−6802.
(44) Hohenberg, P.; Kohn, W. Inhomogeneous Electron Gas. *Phys. Rev.* **1964**, *136*, B864.
(45) Kohn, W.; Sham, L. J. Self-Consistent Equations Including Exchange and Correlation Effects. *Phys. Rev.* **1965**, *140*, A1133.
(46) te Velde, G.; Bickelhaupt, F. M.; Baerends, E. J.; Fonseca Guerra, C.; van Gisbergen, S. J. A.; Snijders, J. G.; Ziegler, T. Chemistry with ADF. *J. Comput. Chem.* **2001**, *22*, 931−967.
(47) Perdew, J. P.; Burke, K.; Ernzerhof, M. Generalized Gradient Approximation Made Simple. *Phys. Rev. Lett.* **1996**, *77*, 3865.
(48) Hammer, B.; Hansen, L. B.; Nørskov, J. K. Improved Adsorption Energetics within Density-Functional Theory Using Revised Perdew-Burke-Ernzerhof Functionals. *Phys. Rev. B* **1999**, *59*, 7413−7421.
(49) Chong, D. P. Completeness Profiles of One-Electron Basis Sets. *Can. J. Chem.* **1995**, *73*, 79−83.
(50) Van Lenthe, E.; Baerends, E. J. Optimized Slater-Type Basis Sets for the Elements 1−118. *J. Comput. Chem.* **2003**, *24*, 1142−1156.
(51) Klamt, A. Conductor-like Screening Model for Real Solvents: A New Approach to the Quantitative Calculation of Solvation Phenomena. *J. Chem. Phys.* **1995**, *99*, 2224−2235.
(52) Klamt, A.; Jonas, V. Treatment of the Outlying Charge in Continuum Solvation Models. *J. Chem. Phys.* **1996**, *105*, 9972−9981.
(53) Klamt, A.; Schüürmann, G. COSMO: A New Approach to Dielectric Screening in Solvents with Explicit Expressions for the Screening Energy and Its Gradient. *J. Chem. Soc., Perkin Trans. 2* **1993**, 799−805.
(54) Pye, C. C. Ziegler, An Implementation of the Conductor-Like Screening Model of Solvation within the Amsterdam Density Functional Package. *Theor. Chem. Acc.* **1999**, *101*, 396−408.
(55) Buergi, H. B.; Dunitz, J. D. From Crystal Statics to Chemical Dynamics. *Acc. Chem. Res.* **1983**, *16*, 153−161.
(56) Murray-Rust, P.; Buergi, H. B.; Dunitz, J. D. Chemical Reaction Paths. V. SN1 Reaction of Tetrahedral Molecules. *J. Am. Chem. Soc.* **1975**, *97*, 921−922.
(57) Coppens, P. Molecular Excited State Structure by Time-Resolved Pump-Probe X-ray Diffraction. What is New and What are the Prospects for Further Progress ? *J. Phys. Chem. Lett.* **2011**, *2*, 616−621.
(58) Howard, J. A. K.; Probert, M. R. Cutting-Edge Techniques Used for the Structural Investigation of Single Crystals. *Science* **2014**, *343*, 1098−1102.
(59) Leblanc, M.; Tressaud, A. In *Comprehensive Inorganic Chemistry II*, 2nd ed.; Reedijk, J., Poeppelmeier, K., Eds.; Elsevier: Amsterdam, 2013; p 161.

DOI: 10.1021/jp5117189
J. Phys. Chem. C 2015, 119, 3322−3330

(60) Constable, E. C.; Cargill Thompson, A. M. W. Ligand Reactivity in Iron(II) Complexes of 4′-(4‴-Pyridyl)-2,2′:6′,2″-terpyridine. *J. Chem. Soc., Dalton Trans.* **1992**, 2947−2950.
(61) Constable, E. C.; Smith, D. R. 4′-(9-Anthryl)-2,2′:6′,2″-terpyridine—a Novel Luminescent Component for Metallosupramolecular Systems. *Supramol. Chem.* **1994**, *4*, 5−7.
(62) Constable, E. C.; Davies, J. E.; Phillips, D.; Raithby, P. R. Coordination Chemistry of 5,5″-Disubstituted 2,2′:6′,2″-Terpyridines. *Polyhedron* **1998**, *17*, 3989−3997.
(63) Constable, E. C.; Baum, G.; Bill, E.; Dyson, R.; van Eldik, R.; Fenske, D.; Kaderli, S.; Morris, D.; Neubrand, A.; Neuburger, M.; et al. Control of Iron(II) Spin States in 2,2′:6′,2″-Terpyridine Complexes through Ligand Substitution. *Chem.—Eur. J.* **1999**, *5*, 498−508.
(64) Pelascini, F.; Wesolek, M.; Peruch, F.; De Cian, A.; Kyritsakas, N.; Lutz, P. J.; Kress, J. Iron Complexes of Terdentate Nitrogen Ligands: Formation and X-ray Structure of Three New Dicationic Complexes. *Polyhedron* **2004**, *23*, 3193−3199.
(65) Brauchli, S. Y.; Constable, E. C.; Harris, K.; Haussinger, D.; Housecroft, C. E.; Rosel, P. J.; Zampese, J. A. Towards Catenanes Using pi-Stacking Interactions and their Influence on the Spin-State of a bis(2,2′:6′,2″-terpyridine) Iron(II) Domain. *Dalton Trans.* **2010**, *39*, 10739−10748.
(66) Baker, A. T.; Goodwin, H. A. Crystal-Structure of Bis(2,2′-6′,2″-terpyridine)Iron(II) bis(perchlorate) Hydrate. *Aust. J. Chem.* **1985**, *38*, 207−214.
(67) Laine, P.; Gourdon, C. A.; Launay, J.-P. Chemistry of Iron with Dipicolinic Acid. 4. Mixed-Ligand Complexes of Iron(III) and Related Compounds. *Inorg. Chem.* **1995**, *34*, 5156−5165.
(68) Constable, E. C.; Ward, M. D. A Convenient, High Yield Synthesis of 2,2′:6′,2″-Terpyridine and Its Iron(II) Complex. *Inorg. Chim. Acta* **1988**, *141*, 201−203.
(69) Adamson, A. W. In *Inorganic Compounds with Unusual Properties*; American Chemical Society: Washington, DC, 1976; Vol. *150*, p 128.
(70) Adamson, A. W. *J. Phys. Chem.* **1967**, *71*, 798.
(71) Medlycott, E. A.; Hanan, G. S. Designing Tridentate Ligands for Ruthenium(II) Complexes with Enhanced Room Temperature Luminescence Lifetimes. *Chem. Soc. Rev.* **2005**, *34*, 133−142.
(72) Medlycott, E. A.; Hanan, G. S. Synthesis and Properties of Mono- and Oligo-Nuclear Ru(II) Complexes of Tridentate Ligands: the Quest for Long-Lived Room Temperature Excited States. *Coord. Chem. Rev.* **2006**, *250*, 1763−1782.
(73) Brown, D. G.; Sanguantrakun, N.; Schulze, B.; Schubert, U. S.; Berlinguette, C. P. Bis(tridentate) ruthenium-terpyridine Complexes Featuring Microsecond Excited-State Lifetimes. *J. Am. Chem. Soc.* **2012**, *134*, 12354−12357.
(74) Mercs, L.; Albrecht, M. Beyond Catalysis: N-heterocyclic Carbene Complexes as Components for Medicinal, Luminescent, and Functional Materials Applications. *Chem. Soc. Rev.* **2010**, *39*, 1903−1912.
(75) Son, S. U.; Park, K. H.; Lee, Y.-S.; Kim, B. Y.; Choi, C. H.; Lah, M. S.; Jang, Y. H.; Jang, D.-J.; Chung, Y. K. Synthesis of Ru(II) Complexes of N-heterocyclic Carbenes and their Promising Photoluminescence Properties in Water. *Inorg. Chem.* **2004**, *43*, 6896−6898.
(76) Ferrere, S. New Photosensitizers Based upon $[Fe(L)_2(CN)_2]$ and $[Fe(L)_3]$ (L = Substituted 2,2′-Bipyridine): Yields for the Photosensitization of TiO_2 and Effects on the Band Selectivity. *Chem. Mater.* **2000**, *12*, 1083−1089.
(77) Ferrere, S. New Photosensitizers Based Upon $[FeII(L)_2(CN)_2]$ and $[FeIIL_3]$, where L Is Substituted 2,2′-Bipyridine. *Inorg. Chim. Acta* **2002**, *329*, 79−92.
(78) Xia, H.-L.; Ardo, S.; Narducci Sarjeant, A. A.; Huang, S.; Meyer, G. J. Photodriven Spin Change of Fe(II) Benzimidazole Compounds Anchored to Nanocrystalline TiO_2 Thin Films. *Langmuir* **2009**, *25*, 13641−13652.
(79) Liu, Y.; Harlang, T.; Canton, S. E.; Chabera, P.; Suarez-Alcantara, K.; Fleckhaus, A.; Vithanage, D. A.; Goransson, E.; Corani, A.; Lomoth, R.; et al. Towards Longer-Lived Metal-to-Ligand Charge Transfer States of Iron(II) Complexes: an N-heterocyclic Carbene Approach. *Chem. Commun.* **2013**, *49*, 6412−6414.
(80) Fredin, L. A.; Pápai, M.; Rozsályi, E.; Vankó, G.; Wärnmark, K.; Sundström, V.; Persson, P. Exceptional Excited-State Lifetime of an Iron(II)−N-Heterocyclic Carbene Complex Explained. *J. Phys. Chem. Lett.* **2014**, *5*, 2066−2071.
(81) Purcell, K. F. Pseudorotational Intersystem Crossing in d^6 Complexes. *J. Am. Chem. Soc.* **1979**, *101*, 5147−5152.
(82) Deeth, R. J.; Anastasi, A. E.; Wilcockson, M. J. An In Silico Design Tool for Fe(II) Spin Crossover and Light-Induced Excited Spin State-Trapped Complexes. *J. Am. Chem. Soc.* **2010**, *132*, 6876−6877.
(83) Lundberg, M.; Kroll, T.; DeBeer, S.; Bergmann, U.; Wilson, S. A.; Glatzel, P.; Nordlund, D.; Hedman, B.; Hodgson, K. O.; Solomon, E. I. Metal−Ligand Covalency of Iron Complexes from High-Resolution Resonant Inelastic X-ray Scattering. *J. Am. Chem. Soc.* **2013**, *135*, 17121−17134.
(84) Benson, C. R.; Hui, A. K.; Parimal, K.; Cook, B. J.; Chen, C.-H.; Lord, R. L.; Flood, A. H.; Caulton, K. C. Multiplying the Electron Storage Capacity of a Bis-tetrazine Pincer Ligand. *Dalton Trans.* **2014**, *43*, 6513−6524.
(85) Dixon, I. M.; Alary, F.; Boggio-Pasqua, M.; Heully, J. L. The $(N_4C_2)^{2-}$ Donor Set as Promising Motif for Bis(tridentate) Iron(II) Photoactive Compounds. *Inorg. Chem.* **2013**, *52*, 13369−13374.
(86) Abrahamsson, M.; Jäger, M.; Österman, T.; Eriksson, L.; Persson, P.; Becker, H.-C.; Johansson, O.; Hammarström, L. Bistridentate Ruthenium(II)polypyridyl-Type Complexes with Microsecond ^{3}MLCT State Lifetimes: Sensitizers for Rod-Like Molecular Arrays. *J. Am. Chem. Soc.* **2006**, *128*, 12616−12617.
(87) Abrahamsson, M.; Jäger, M.; Kumar, R. J.; Österman, T.; Persson, P.; Becker, H.-C.; Johansson, O.; Hammarström, L. Bistridentate Ruthenium(II)polypyridyl-Type Complexes with Microsecond ^{3}MLCT State Lifetimes: Sensitizers for Rod-Like Molecular Arrays. *J. Am. Chem. Soc.* **2008**, *130*, 15533−15542.
(88) Jamula, L. L.; Brown, A. M.; Guo, D.; McCusker, J. K. Synthesis and Characterization of a High-Symmetry Ferrous Polypyridyl Complex: Approaching the $^5T_2/^3T_1$ Crossing Point for Fe^{II}. *Inorg. Chem.* **2013**, *53*, 15−17.
(89) Craig, G. A.; Barrios, L. A.; Costa, J. S.; Roubeau, O.; Ruiz, E.; Teat, S. J.; Wilson, C. C.; Thomas, L.; Aromi, G. Synthesis of a Novel Heptacoordinated Fe(III) Dinuclear Complex: Experimental and Theoretical Study of the Magnetic Properties. *Dalton Trans.* **2010**, *39*, 4874−4881.
(90) Craig, G. A.; Sánchez Costa, J.; Roubeau, O.; Teat, S. J.; Aromí, G. Coupled Crystallographic Order-Disorder and Spin State in a Bistable Molecule: Multiple Transition Dynamics. *Chem.—Eur. J.* **2011**, *17*, 3120−3127.
(91) Craig, G. A.; Costa, J. S.; Teat, S. J.; Roubeau, O.; Yufit, D. S.; Howard, J. W. K.; Aromí, G. Multimetastability in a Spin-Crossover Compound Leading to Different High-Spin-to-Low-Spin Relaxation Dynamics. *Inorg. Chem.* **2013**, *52*, 7203−7209.
(92) Huang, J.; Buyukcakir, O.; Mara, M. W.; Coskun, A.; Dimitrijevic, N. M.; Barin, G.; Kokhan, O.; Stickrath, A. B.; Ruppert, R.; Tiede, D. M.; et al. Highly Efficient Ultrafast Electron Injection from the Singlet MLCT Excited State of Copper(I) Diimine Complexes to TiO_2 Nanoparticles. *Angew. Chem., Int. Ed.* **2012**, *51*, 12711−12715.

DOI: 10.1021/jp5117189
J. Phys. Chem. C 2015, 119, 3322−3330